Applied Catalysis B: Environmental 129 (2013) 153–162

Contents lists available at SciVerse ScienceDirect

Applied Catalysis B: Environmental

journal homepage: www.elsevier.com/locate/apcatb

Sulfate radicals induced degradation of tetrabromobisphenol A with nanoscaled magnetic $CuFe_2O_4$ as a heterogeneous catalyst of peroxymonosulfate

Yaobin Ding[a,b], Lihua Zhu[a], Nan Wang[a,b], Heqing Tang[b,*]

[a] College of Chemistry and Chemical Engineering, Huazhong University of Science and Technology, Wuhan 430074, PR China
[b] Key Laboratory of Catalysis and Materials Science of the State Ethnic Affairs Commission and Ministry of Education, College of Chemistry and Material Science, South-Central University for Nationalities, Wuhan 430074, PR China

ARTICLE INFO

Article history:
Received 25 June 2012
Received in revised form 10 August 2012
Accepted 12 September 2012
Available online 18 September 2012

Keywords:
Tetrabromobisphenol A
Oxidative degradation
Peroxymonosulfate
$CuFe_2O_4$
Sol–gel combustion method

ABSTRACT

$CuFe_2O_4$ magnetic nanoparticles (MNPs) were prepared by sol–gel combustion method with copper and iron nitrates as metal precursors and citrate acid as a complex agent. The obtained $CuFe_2O_4$ MNPs were characterized by scanning electron microscopy, X-ray diffractometry, Fourier transform infrared spectroscopy, Fourier transform Raman spectroscopy and X-ray photoelectron spectroscopy. It was found that $CuFe_2O_4$ MNPs could effectively catalyze peroxymonosulfate (PMS) to generate sulfate radicals ($SO_4^{\bullet -}$) to degrade tetrabromobisphenol A (TBBPA). The added TBBPA (10 mg L^{-1}) was almost completely removed (with a removal of 99%) in 30 min by using 0.1 g L^{-1} $CuFe_2O_4$ MNPs and 0.2 mmol L^{-1} PMS. With higher addition of PMS (1.5 mmol L^{-1}), the degradation yielded a TOC removal of 56% and a TBBPA debromination ratio of 67%. The effect of catalyst calcination temperature, catalyst load, PMS concentration and reaction temperature was investigated on the catalytic activity of $CuFe_2O_4$ MNPs. The highly catalytic activity of $CuFe_2O_4$ MNPs possibly involved the activation of PMS by both Cu(II) and Fe(III) in $CuFe_2O_4$ MNPs. Based on intermediate detections, the degradation pathway of TBBPA in the $CuFe_2O_4$ MNPs/PMS system was proposed.

1. Introduction

Tetrabromobisphenol A (TBBPA) is a well-known brominated flame retardant, which has been widely utilized in the treatment of paper, textiles, plastics, electronic equipment and upholstered furniture [1]. Due to its widespread use and the lipophilicity, TBBPA and its dimethylated derivative have been detected in various environmental matrices, including sediment near manufacturing facilities and mussels [2], sewage sludge [3] or air at the dismantling plant [4]. As an endocrine disruptor, they have been found to negatively affect various aspects of mammalian and human physiology [5,6]. Therefore, developing effective methods to removal TBBPA from the contaminated environment is of necessity and importance.

The treatment of TBBPA was reported through different processes [7–14]. Voordeckers et al. investigated the biodegradation kinetics of several brominated flame retardants in aerobic and anaerobic soil and calculated the half-life of TBBPA in aerobic soil to be 65 days in the experiment with activated sludge and as long as 93 days in the experiment with digested sludge [7]. It is certain that the biodegradation kinetics of TBBPA is slow. TBBPA could be degraded under UV irradiation [13], by δ-MnO_2 oxidation [8] and photosensitized oxidation [11,12], but it was accompanied with the generation of brominated isopropylphenol derivatives as major degradation products, which may have greater potential threats to aqueous environment [15]. By using mesoporous BiOBr as the photocatalyst, the photocatalytic oxidation of TBBPA was fast with a degradation removal of almost 100% after 15 min, but the TOC value of the TBBPA solution was decreased by only 15% after 120 min irradiation in this system [10]. Because the difficulty in the oxidative debromination of TBBPA, a "two-stage reduction subsequent oxidation" process consisting of Fe–Ag reduction and Fenton-like oxidation under ultrasound radiation was used to remove TBBPA by combining reductive debromination and successive oxidation [14]. At the present time, more effective methods with high debromination and TOC removal are needed to be developed to remove TBBPA from the contaminated environment.

Sulfate radical based advanced oxidation technologies have become a hotspot due to its high oxidizing ability. Sulfate radicals can be generated by activation of persulfate or PMS by UV, heat and transition metal [16–18]. Among the tested transition metals including Ag(I), Ce(III), Co(II), Fe(II), Fe(III), Mn(II), Ni(II), Ru(III) and

* Corresponding author. Tel.: +86 27 67843323; fax: +86 27 67843323.
E-mail address: hqtang62@yahoo.com.cn (H. Tang).

0926-3373/$ – see front matter © 2012 Elsevier B.V. All rights reserved.
http://dx.doi.org/10.1016/j.apcatb.2012.09.015

V(III), Co(II) is the most effective catalyst of PMS activation for the production of sulfate radicals according to the following reaction [18].

$$M^{n+} + HSO_5^- \rightarrow M^{(n+1)} + SO_4^{\bullet -} + OH^- \quad (1)$$

Anipsitakis and Dionysiou used the homogeneous Co(II)/PMS system to treat 2,4-dichlorophenol, naphthalene and atrazine in solutions at pH 3–8, and found that the sulfate radicals based system yielded higher TOC removal than the Fenton process [19]. This homogeneous Co(II)/PMS system was also applied for the degradation of azo dyes [20,21], phenolic pollutants [22,23] and other pollutants [24,25]. However, the toxicity of Co ion limited its applications in practical environmental protection [26]. To decrease the use of dissolved Co(II), two ways were tried: (1) developing heterogeneous Co-bearing catalysts and (2) substituting other transition metals for Co(II). Indeed, cobalt leaching was reduced by the use of heterogeneous Co-bearing catalysts including Co_3O_4 nanoparticle [27,28] and its immobilization on various metal oxides supports such as TiO_2 [29], SBA-15 [30], MgO [31], zeolite [32], activated carbon [33], carbon aerogel [34], graphene oxide [35,36], coal fly ash [37] and other materials [38–40]. We found that the composition of Co_3O_4 with Bi_2O_3 enhanced its reactivity for the degradation of organic pollutants and decreased the cobalt leaching from 158 to 43 $\mu g\,L^{-1}$ [38]. As the second way, Rastogi et al. used Fe(II) and Fe(III) as an activator of PMS for the PCBs degradation in aqueous and sediment systems and found that the Fe(II)/PMS system was effective in degrading PCB in a sediment–slurry system with more than 90% PCB removal within 24 h [41]. Wang et al. used the Fe(II)/PMS and UV-Fe(II)/PMS systems for the degradation of a xanthene dye Rhodamine B and 2,4,5-trichlorophenoxyacetic acid in aqueous solution [42,43]. In addition, Cu(II) also presented PMS activation ability to generate sulfate radicals for the degradation of azo dye acid red 88 and triclosan [44,45]. Ji et al. reported a fast degradation of phenol ($50\,mg\,L^{-1}$) by using CuO particles ($1.5\,g\,L^{-1}$) to activate PMS ($1.5\,mmol\,L^{-1}$) at pH 4.0 [46].

Spinel ferrites with the formula of MFe_2O_4, where M represents a divalent metal (such as Cu, Mn, Mg and Zn) have attracted extensive attention due to their potential applications including magnetic recording media, magnetic resonance imaging, magnetically guided drug delivery, and sensors due to their unique optical, electrical and magnetic properties [47]. As one of spinel ferrites, $CuFe_2O_4$ was usually used as a catalyst in the decomposition of gaseous pollutants [48], water gas shift reaction [49] and hydrogen production from oxygenated hydrocarbons [50]. Because $CuFe_2O_4$ MNPs have both Cu and Fe elements, we anticipated $CuFe_2O_4$ MNPs as a powerful candidate for the catalytic activation of PMS. Therefore, $CuFe_2O_4$ MNPs were prepared by sol–gel combustion method and used as catalysts to generate sulfate radicals. The present work is aimed at investigating the effectiveness and feasibility of such a system in treatment of TBBPA. The activation mechanism of PMS by $CuFe_2O_4$ MNPs and the degradation pathway of TBBPA in such a system were also proposed. To the best of our knowledge, this is the first try to use $CuFe_2O_4$ MNPs as a catalyst of PMS for the degradation of TBBPA.

2. Materials and methods

2.1. Chemicals

Cupric nitrate ($Cu(NO_3)_2{\cdot}3H_2O$), ferric nitrate ($Fe(NO_3)_3{\cdot}9H_2O$), citric acid, sodium hydroxide and hydrochloric acid were provided by Sinopharm Chemical Reagent Co., Ltd (Shanghai, China). Oxone ($2KHSO_5{\cdot}KHSO_4{\cdot}K_2SO_4$, 4.7% active oxygen) was purchased from Shanghai D&R Finechem Co., Ltd (Shanghai, China). TBBPA was purchased from Sigma–Aldrich Company. TBBPA stock solution ($4\,g\,L^{-1}$) was prepared by dissolving 0.4 mg TBBPA in 100 mL of $0.1\,mol\,L^{-1}$ NaOH solution. All chemicals were analytical grade reagents and were used as received without further purification. Double distilled water was used in the present work.

2.2. Preparation of $CuFe_2O_4$, CuO and Fe_2O_3 nanoparticles

$CuFe_2O_4$ MNPs were prepared by sol–gel combustion method based on citrate complexation as reported on the literature [51,52]. In this method, different cations can effectively be accommodated in the complex, leading to uniform mixing of the cations [53]. An aqueous solution of $Cu(NO_3)_2{\cdot}3H_2O$ (0.005 mol) and $Fe(NO_3)_3{\cdot}9H_2O$ (0.01 mol) was stirred at 60 °C for 2 h, and then citric acid was added until the molar ratio of citric acid to the total metal cations was unity. The resultant homogeneous solution was stirred for another 2 h at 60 °C, and then heated to 90 °C to evaporate water. The obtained nitrate–citrate complex gel was heated at a given temperature (typically at 400 °C) for 2 h to decompose citric acid until fine oxide powders were obtained. For a comparison, CuO and Fe_2O_3 nanoparticles with the comparable particle size with that of $CuFe_2O_4$ MNPs were also prepared by the same method by individually using $Cu(NO_3)_2$ and $Fe(NO_3)_3$ as a precursor, respectively, but with calcination at 400 °C for 1 h.

2.3. Catalytic degradation experiment

Unless otherwise specified, the degradation experiments were carried out in a 100 mL reactor at 25 °C (Fig. S1 in Supporting Information). $CuFe_2O_4$ MNPs ($0.1\,g\,L^{-1}$) were firstly dispersed into 100 mL aqueous solution of $10\,mg\,L^{-1}$ TBBPA by sonication for 1 min. The suspension was mechanically stirred in dark for 20 min to achieve the adsorption/desorption equilibrium between the TBBPA solution and the catalyst. Then, a specified amount of PMS in the form of Oxone was added into the solution to initiate the reaction and the pH value declined from 8.2 to 7.1 due to the acidity of Oxone. When the degradation process of TBBPA was finished, the final pH value was about 6.3. After the degradation was initiated, solution samples (1.0 mL) were taken at given time intervals during the reaction, and immediately filtered with 0.2 μm filter into a HPLC vial. Before the filtrating, 0.5 mL of ethanol solution was immediately added to quench the reaction. The concentration of residual TBBPA was analyzed by using a HPLC, along with the determination of generated Br^- by using ion chromatography.

Two sets of quenching experiments were performed to determine the radical species formed in the $CuFe_2O_4$/PMS/TBBPA system by using *tert*-butyl alcohol (TBA) and ethanol (EtOH) as the quenching agents, respectively. As we know, EtOH is widely used as a scavenger of hydroxyl and sulfate radicals, while TBA is an effective quenching agent for hydroxyl radicals. Prior to the addition of $CuFe_2O_4$ and PMS, a required amount of the alcohol quencher was added into the reaction solution to obtain a concentration of $100\,mmol\,L^{-1}$, corresponding to 500:1 for the molar ratio of alcohol to PMS.

To test the stability and recyclability of catalysts, after the added TBBPA was almost completely degraded, the used catalyst was collected by vacuum filtration, washed with water to neutral pH, and dried at 60 °C for 8 h. The recycled catalyst was re-dispersed into a fresh solution of TBBPA, and the TBBPA degradation was re-initiated by adding the same concentration of PMS. This catalyst recycling and the degradation experiment were repeated five times. After used five times, the $CuFe_2O_4$ MNPs catalyst was recycled, dried and divided into two parts. One part was dissolved by $1\,mol\,L^{-1}$ HCl, and Cu and Fe concentration in the dissolved solution was determined by AAS to investigate the bulky chemical composition. The other part was for the surface element composition analysis by XPS. All measurements were repeated three times

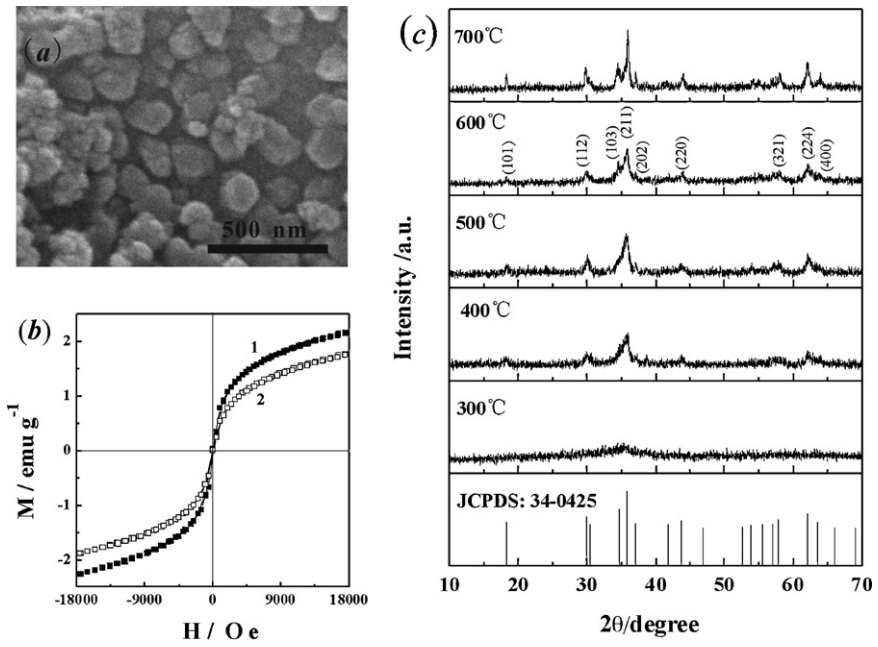

Fig. 1. Characterization of $CuFe_2O_4$ MNPs. (a) SEM image of the sample calcined at 400 °C, (b) *M–H* hysteresis loops of (1) fresh $CuFe_2O_4$ MNPs and (2) used $CuFe_2O_4$ MNPs after being used five times at 300 K. (c) XRD patterns of the samples calcined at different temperatures.

and the results were reproducible within the experimental errors (±5%).

2.4. Characterization

The surface morphology was characterized on a Quanta 200 scanning electron microscopic (SEM) instrument (FEI, the Netherlands). X-ray powder diffraction (XRD) pattern was obtained on a diffractometer with Cu K_α radiation (PANalytical B.V. X'Pert PRO), operated at 40 mA and 40 kV. FT-IR spectra were recorded on a Bruker VERTEX 70 spectrometer. Raman spectrum was measured by a confocal laser micro-Raman spectrometer (DXR, USA) equipped with a He–Ne laser of excitation of 532 nm at a laser power of 0.6 mW. The element composition and chemical oxidation state were investigated by X-ray photoelectron spectra (XPS) on a VG Multilab 2000 spectrometer (Thermo Electron Corporation) with Al K_α radiation as the exciting source (300 W). Binding energies were calibrated versus the carbon signal at 284.64 eV. The magnetic properties (*M–H* curve) were measured at 300 K on an ADE 4HF vibrating sample magnetometer.

2.5. Chemical analysis

TBBPA concentration was measured by using a HPLC with a UV detector at a wavelength of 230 nm. An amethyst C18-P column (5 μm, 120 Å; 4.6 × 250 mm) was used as separation column. The mobile phase used for HPLC experiments was a mixture of methanol and water (85:15, v/v) and was filtered through 0.2 μm filter prior to use. The flow rate was set at 1.0 mL min^{-1} and the injection volume was 50 μL. The calibration curve indicated a good linear correlation for TBBPA concentrations in the range of 0.1–20 mg L^{-1} (R = 0.999), with detection limit (S/N = 3) of 0.033 mg L^{-1} (Fig. S2 in Supporting Information).

The concentration of Br^- was monitored on a Metrohm 792 ion chromatography system equipped with the CD 25 conductivity detector, IonPac AS 23 (250 mm × 4 mm) analytical column, IonPac AG 23 (50 mm × 4 mm) guard column, and anion ASRS electrolytic suppressor (ASRS-ULTRA II, 4 mm, suppressor current of 70 mA). The mobile phase was 28 mmol L^{-1} Na_2CO_3–$NaHCO_3$ with a flow rate of 1.0 mL min^{-1}, and the injection volume was 20 μL.

For reaction product identification, 40 mg L^{-1} TBBPA and 0.1 g L^{-1} $CuFe_2O_4$ MNPs were mixed in 100 mL reaction solution and the reaction was started by the addition of 1.0 mmol L^{-1} PMS. 2.0 ml solution samples were taken after 40 min reaction, quenched by 1 mL ethanol solution and immediately filtered with 0.2 μm filter into a HPLC vial before chemical structure analysis by LC–MS. The brominated degradation intermediate products of TBBPA were monitored by the mass spectrometer (Agilent 1100 LC/MSD Trap, USA) in electrospray negative ion (ESI^-) mode with methanol and water (85:15, v/v). The aromatic products and organic acids were identified by the mass spectrometer (Agilent 1100 LC/MSD Trap, USA) in electrospray positive ion (ESI^+) mode with more polar elute of methanol and water (5:95, v/v).

Total organic carbon (TOC) was assayed by using TOC analyzer micro N/C model (Analytik Jena, Germany). The Cu ion leaching was monitored by atomic absorption spectroscopy (AAS, Analyst 300, P.E. Inc.). The Fe ion leaching was detected with inductively coupled plasma-atomic emission spectroscopy (ICP-AES; Baird Plasma Spectrovac PS-6(N + 1)).

3. Results and discussion

3.1. Characterization of catalysts

The prepared $CuFe_2O_4$ MNPs were characterized as shown in Figs. 1 and 2. The SEM observation showed that $CuFe_2O_4$ MNPs were composed of quasi-sphere particles with particle sizes of about 100 nm (Fig. 1a), being comparable with particle size of CuO and Fe_2O_3 catalysts (about 100 nm in diameter, Fig. S3 in Supporting Information). The *M–H* curve of fresh $CuFe_2O_4$ MNPs (Fig. 1b) demonstrated that the saturation moment per unit mass was about 2.2 emu g^{-1}. In Fig. 1c, the XRD pattern of $CuFe_2O_4$ MNPs calcined at 400 °C presented three intense diffraction peaks at 2θ angle of 34.718°, 35.861° and 62.156°, being well matched with the published JCPDS data (JCPDS File No. 34-0425) for the tetragonal $CuFe_2O_4$ spinel [52]. These reflections became shaper with increasing calcination temperature, indicative of the development of crystalline structures. Based on the XRD peak, the grain size was calculated with Sherrer equation as 15.3, 26.6 and 25.0 nm for $CuFe_2O_4$, CuO and Fe_2O_3 crystals calcined at 400 °C,

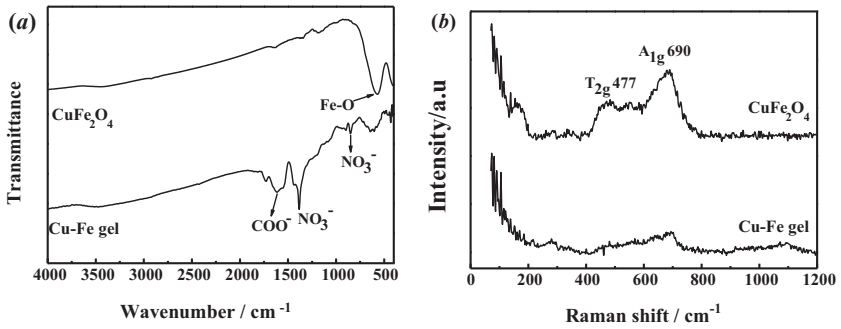

Fig. 2. (a) FT-IR and (b) Raman spectra of Cu–Fe gel and $CuFe_2O_4$ samples calcined at 400 °C.

respectively, being much smaller than their corresponding particle sizes as signed by the broad XRD peak.

Fig. 2 showed the FT-IR and Raman spectra of the $CuFe_2O_4$ MNP samples before and after the calcination treatment. The FT-IR spectra (Fig. 2a) verified the formation of Fe—O bond in the tetrahedral FeO_6 groups of spinel-type compounds, corresponding to the absorption band around 570 cm^{-1} [52]. By comparing the $CuFe_2O_4$ MNPs with and without calcination, the disappearance of absorption bands in the frequency range 1600–1400 cm^{-1} and 1440–1350 cm^{-1} being indicative of the asymmetric and symmetric COO^- stretching vibrations of the citrate ligands and the existence of NO_3^- demonstrated the complete removal of organic residues after being calcined at 400 °C [54]. In the Raman spectra (Fig. 2b), the strong band at 690 cm^{-1} for A_{1g} stretching vibration of Fe—O bond in the tetrahedral FeO_6 groups of $CuFe_2O_4$ MNPs was observed by the Raman analysis (Fig. 2b), which was consistent with the FT-IR results [55].

The contents of Cu and Fe in the as-prepared catalyst were measured by AAS to investigate the bulky chemical composition of the catalyst. It was found that the atomic ratio of Cu to Fe was equal to 1:2 in the $CuFe_2O_4$ MNPs sample, which is rational because both the Cu and Fe precursors were added with the molar ratio of 1:2.

3.2. High catalytic activity of $CuFe_2O_4$ MNPs

Fig. 3 gave the kinetic data of TBBPA degradation in different systems. The addition of PMS (0.2 mmol L^{-1}) in the absence of any catalyst brought about only 4% of TBBPA removal in 30 min, and the addition of $CuFe_2O_4$ MNPs (0.1 g L^{-1}) alone enhanced the TBBPA degradation little. However, it was found that $CuFe_2O_4$, Fe_2O_3 and CuO nanoparticles were able to be used as catalyst for the activation of PMS. The simultaneous use of $CuFe_2O_4$ MNPs and PMS promoted the TBBPA degradation significantly, yielding a TBBPA removal of 99% in 30 min, which was higher than the TBBPA removal of 66% and 85% achieved by adding Fe_2O_3 and CuO particles as the catalyst, respectively.

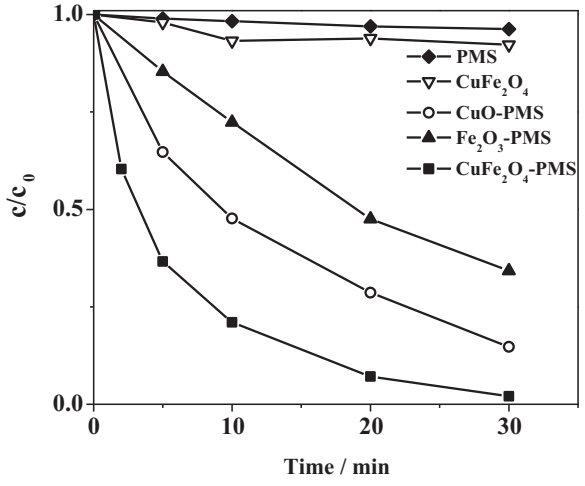

Fig. 3. Degradation kinetics of TBBPA in different systems. Reaction conditions: initial TBBPA concentration 10 mg L^{-1}, initial PMS concentration 0.2 mmol L^{-1}, and catalyst load 0.1 g L^{-1}.

Under all the tested conditions, the TBBPA degradation approximately followed a pseudo first order reaction in kinetics, which may be expressed as $\ln(c_t/c_0) = -kt$, where t is reaction time (min), k is the apparent rate constant (min^{-1}), and c_0 and c_t are pollutant concentrations (μmol L^{-1}) at time of $t = 0$ and $t = t$, respectively. The k values of TBBPA degradation with an initial concentration of 10 mg L^{-1} were evaluated as 0.036, 0.061 and 0.12 min^{-1} for the catalysts of Fe_2O_3, CuO and $CuFe_2O_4$ nanoparticles, respectively. The superior catalytic activity of $CuFe_2O_4$ MNPs may be ascribed to the synergy effect of Cu and Fe active site on the $CuFe_2O_4$ MNPs surface.

To clarify whether the catalytic degradation of TBBPA was conducted heterogeneously over $CuFe_2O_4$ MNPs catalyst surface or homogeneously by dissolved Cu^{2+} and/or Fe^{3+} ions, the leaching solution was obtained by vacuum filtration after the TBBPA degradation experiment. Only 8% of TBBPA removal was observed by the leaching solution with the addition of 0.2 mmol L^{-1} PMS, being much lower than that (99% removal) in the system of PMS/$CuFe_2O_4$. This indicates that the degradation process of TBBPA is heterogeneously conducted on the surface of $CuFe_2O_4$ MNPs catalyst.

3.3. Effect of several parameters on catalytic activity of $CuFe_2O_4$ MNPs

The effect of calcination temperature in the range of 100–700 °C on the catalytic activity of $CuFe_2O_4$ MNPs and Cu^{2+} leaching was investigated in the presence of 0.1 g L^{-1} $CuFe_2O_4$ MNPs and 0.2 mmol L^{-1} PMS. As shown in Fig. 4a, the catalytic performance of the catalyst was initially enhanced and then decreased as the calcination temperature was elevated. For example, the as-prepared Cu–Fe gel showed no reaction activity for the TBBPA degradation. After the calcination treatment at 200 °C, the catalytic performance was enhanced with the apparent rate constant k of 1.14×10^{-2} min^{-1} due to the partial decomposition of citric acid in the as-prepared Cu–Fe gel [56]. The highest catalytic activity was observed with the sample calcined at 300 °C, at which almost complete removal of TBBPA (100%) was obtained and the apparent rate constant was observed with a rate constant of 0.15 min^{-1}. However, the catalytic performance was decreased with the further increase of the calcination temperature. When the calcination temperature was elevated from 300 to 400 °C, the apparent rate constant k was decreased slightly from 0.15 to 0.12 min^{-1}. Further increasing the calcination temperature to 600 and 700 °C resulted in much smaller k values of 0.05 and 0.03 min^{-1}, respectively.

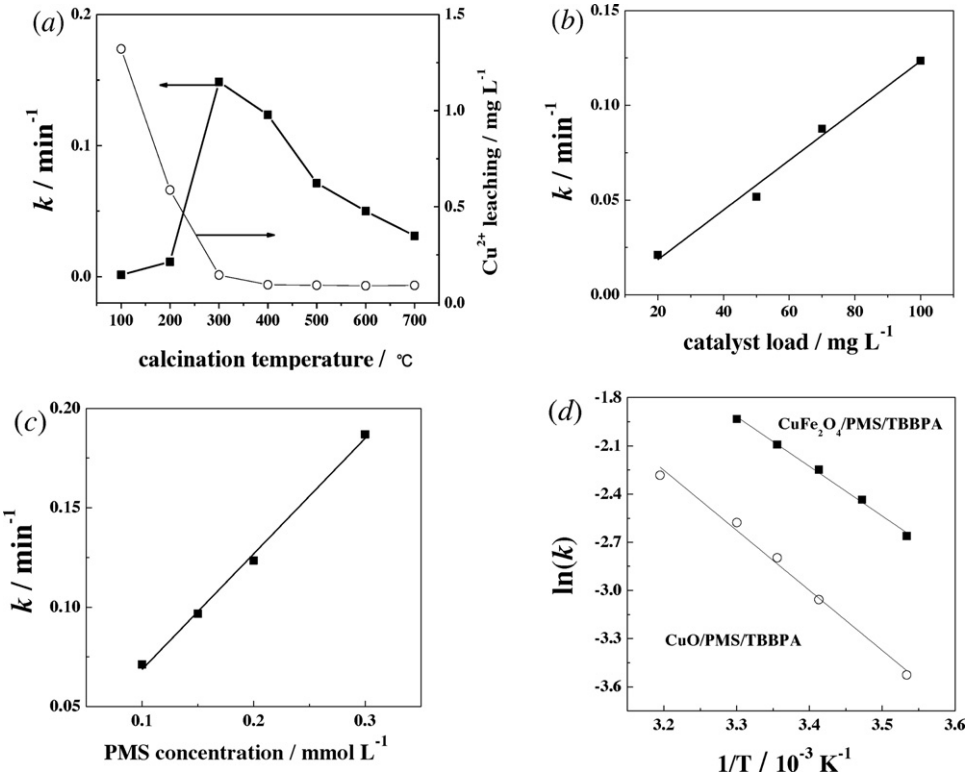

Fig. 4. Effects of (a) calcinations temperature, (b) catalyst load, (c) initial PMS concentration and (d) reaction temperature on the rate constant of TBBPA degradation. The amount of Cu^{2+} leaching was also given in (a).

The adsorption of TBBPA and the evolution of residual PMS were also determined on the $CuFe_2O_4$ MNPs calcined at different temperatures (Fig. S4 in Supporting Information). It was observed that the adsorption amount of TBBPA on the surface of $CuFe_2O_4$ catalyst was decreased from 12% to 8% and further to 4% when the calcination temperature was increased from 300 °C to 400 °C and further to 700 °C. On the other hand, the amount of consumed PMS by $CuFe_2O_4$ catalyst was also decreased with the increase of the calcination temperature (Fig. S4 in Supporting Information). When the calcination temperature was increased from 300 °C to 400 °C and then to 700 °C, the consumption of PMS induced by $CuFe_2O_4$ catalyst in 30 min was decreased from 67%, 52% and 23%, respectively. As shown by the XRD results, calcination treatment induced the crystals to grow in sizes, resulting in decreased specific surface area of $CuFe_2O_4$ MNPs. Therefore, the active sites for the adsorption of TBBPA and the activation of PMS to generate sulfate radicals were also reduced. It is reasonable that slower degradation of TBBPA was observed for the $CuFe_2O_4$ MNPs calcined at higher temperatures.

The heat-treatment also enhanced the stability of $CuFe_2O_4$ MNPs, and decreased the Cu^{2+} and Fe^{3+} leaching from $CuFe_2O_4$ MNPs in the reaction solution. As seen in Fig. 4a, the amount of Cu^{2+} as high as 1.3 mg L^{-1} was dissolved in 120 min for the as-prepared Cu–Fe gel. After the sample was calcined at 200 °C and 300 °C, the amount of dissolved Cu^{2+} was decreased to 0.587 and 0.145 mg L^{-1}, respectively, due to the partial and then complete decomposition of citric acid included in the as-prepared Cu–Fe gel [56]. Upon calcination at elevated temperatures at 400–700 °C, the Cu^{2+} leaching was further reduced to about 0.094 mg L^{-1} due to the formation of spinel $CuFe_2O_4$ phase, which enhances the stability of $CuFe_2O_4$ MNPs confirmed by XRD results shown in Fig. 1c. In addition, Fe^{3+} leaching lower than 0.132 mg L^{-1} was obtained with the catalyst sample calcined at temperature lower than 300 °C, while Fe^{3+} leaching lower than 0.010 mg L^{-1} was observed with the sample calcined at 400–700 °C. Therefore, the calcination temperature to attain the best combination of highly catalytic activity and low Cu^{2+} leaching was fixed at 400 °C.

The effects of $CuFe_2O_4$ MNP load and initial PMS concentration were investigated on the degradation of TBBPA at 25 °C. It was noted that increasing $CuFe_2O_4$ load or initial PMS concentration could promote the degradation of TBBPA (Fig. 4b and c). At the given initial PMS concentration (0.2 mmol L^{-1}), reaction rate constant k was rapidly increased linearly from 0.021 to 0.12 min^{-1} when the catalyst load was increased from 0.02 to 0.1 g L^{-1}. The increased degradation efficiency is evidently attributed to the increased availability of active sites in the solution for reaction with PMS, which will generate more sulfate radicals [57,58]. When the catalyst load was fixed at 0.1 g L^{-1}, the increase of initial PMS concentration also accelerated the removal of TBBPA. The change in PMS concentration from 0.1 to 0.2 and further to 0.3 mmol L^{-1} would increase k value from 0.071 to 0.12 and further to 0.19 min^{-1}. These results suggest that the degradation of TBBPA is enhanced by increasing the catalyst load and PMS concentration.

Fig. 4d depicted the degradation kinetics of TBBPA by PMS in the presence of $CuFe_2O_4$ MNPs at different reaction temperatures. It is clearly seen that reaction temperature significantly affected the degradation rate of TBBPA. At 10 °C, the apparent rate constant k was 0.07 min^{-1} with TBBPA removal of 56% in 30 min, while the k value was increased to 0.12 min^{-1} with TBBPA removal of 99% in 30 min as the temperature was increased to 25 °C. Therefore, the activation energy (E_a) of the oxidative degradation of TBBPA was evaluated by plotting ln$k$ against $1/T$ (Fig. 4d), according to the Arrhenius equation of $\ln k = \ln A - E_a/RT$, where k is the rate constant, R is the universal gas constant (8.314 J mol^{-1} K^{-1}), and A is a constant. The E_a value was evaluated as 25.7 kJ mol^{-1} in the system of $CuFe_2O_4$/PMS/TBBPA. As comparisons, the E_a values in the systems of CuO/PMS/TBBPA, Fe_2O_3/PMS/TBBPA and PMS/TBBPA were obtained as 29.1, 31.1 and 35.9 kJ mol^{-1}, respectively (Fig. S5 in Supporting Information). The lower activation energy on $CuFe_2O_4$

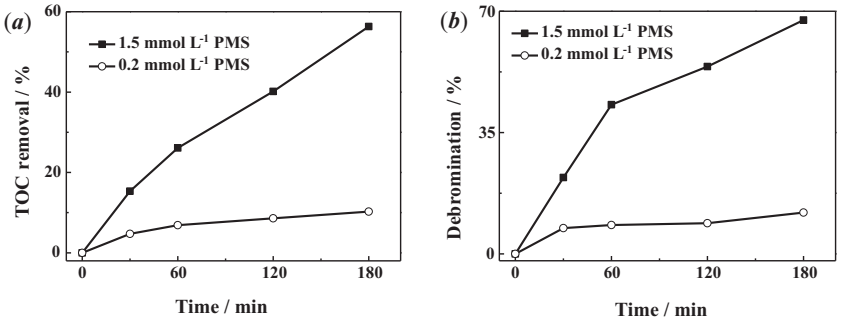

Fig. 5. (a) Removal of TOC and (b) release of Br^- and BrO_3^- during the degradation of TBBPA. Reaction conditions: initial TBBPA concentration 10 mg L^{-1}, initial PMS concentration 0.2 mmol L^{-1} or 1.5 mmol L^{-1}, $CuFe_2O_4$ MNPs load 0.1 g L^{-1}.

MNPs signifies the higher catalytic activity of $CuFe_2O_4$ MNPs in comparison with CuO and Fe_2O_3 catalysts.

3.4. TOC removal and debromination

The degradation process of TBBPA in the presence of PMS and $CuFe_2O_4$ MNPs was monitored by UV–vis spectra (Fig. S6 in Supporting Information). It was found that the strong absorption peak at 310 nm was decreased with the reaction time, indicative of the degradation of TBBPA. Moreover, as the reaction proceeded, the absorption at 207 nm in the UV region attributed to benzene ring also declined, suggesting that TBBPA was mineralized. Therefore, the TOC analysis was carried out to evaluate the mineralization rate of TBBPA in the system of PMS/$CuFe_2O_4$ (Fig. 5a). A TOC removal of 10% was obtained in 180 min in the presence of 0.2 mmol L^{-1} PMS. The mineralization of TBBPA by PMS can be expressed as Eq. (2),

$$C_{15}H_{12}Br_4O_2 + 68\,HSO_5^- \rightarrow 15\,CO_2 + 40\,H_2O + 4\,Br^- + 68\,SO_4^{2-} \quad (2)$$

According to Eq. (2), a complete mineralization of 1 mol L^{-1} TBBPA will consume 68 mol L^{-1} PMS. In the investigated system, the used initial concentration of TBBPA was 10 mg L^{-1}, the complete mineralization of which requires 1.25 mmol L^{-1} PMS. However, only 0.2 mmol L^{-1} PMS was added, which resulted in a TOC removal as low as 10%. Therefore, we added 1.5 mmol L^{-1} PMS to enhance the mineralization of TBBPA, and indeed this caused a TOC removal as high as 56% within 180 min (Fig. 5a).

Corresponding to the two used levels of PMS concentration, the debromination of TBBPA was monitored in the system (Fig. 5b). When 0.2 mmol L^{-1} PMS was added, only Br^- was released and its content was increased with reaction time. After 180 min, 8.8 μmol L^{-1} (0.7 mg L^{-1}) Br^- was observed, which accounted for the debromination ratio of 12% to the added 10 mg L^{-1} TBBPA, matching well with the TOC removal of 10%. When PMS concentration was increased to 1.5 mmol L^{-1}, we detected Br^- and BrO_3^-. The later was due to oxidation of Br^- by generated radicals. In fact, 44.8 μmol L^{-1} of Br^- and 6.4 μmol L^{-1} of BrO_3^- were detected within 180 min as 1.5 mmol L^{-1} PMS was added, which indicated that a TBBPA debromination ratio of 67% was achieved.

3.5. Stability and reusability of $CuFe_2O_4$ MNP catalysts

To evaluate the stability of $CuFe_2O_4$ MNP catalysts, the leaching of Cu^{2+} and Fe^{3+} was measured in the time course of TBBPA degradation with the addition of 0.5 g L^{-1} catalysts, in which the greater catalyst load was used to decrease the possible measurement error (Fig. 6a). It was found that under the reaction conditions, Cu^{2+} leaching was about 94 μg L^{-1} in 120 min, accounting for 0.07% of the total Cu content in the catalyst. ICP-AES analysis indicated that the Fe^{3+} leaching was less than 10 μg L^{-1} under the tested reaction conditions. Moreover, we carried out the degradation process of TBBPA by using the recycled catalysts. After the degradation was finished, the used catalyst was collected by vacuum filtration, washed with water several times to neutral pH, and redispersed in the fresh TBBPA solution. Then, 0.2 mmol L^{-1} PMS was added, and the second cycle of degradation was conducted. These steps were repeated several times. After the fifth run, the TBBPA removal was still about 90% for the catalysts recycled by vacuum filtration, also indicating the excellent stability of $CuFe_2O_4$ MNPs catalyst. Considering the magnetic property of $CuFe_2O_4$ MNPs, we also carried out the batch degradation process of TBBPA by using the catalyst which was recycled with magnetic separation, and found that a TBBPA removal was still as high as 89% in the fifth run (Fig. S7 in Supporting Information). This indicates the feasibility of magnetic separation and further confirms the excellent stability of $CuFe_2O_4$ MNPs catalyst.

After being used for five times, the $CuFe_2O_4$ MNP catalyst was collected by vacuum filtration, dried and divided into two parts. One part was dissolved with 1 mol L^{-1} HCl, and then Cu and Fe concentration in the dissolved solution was determined by AAS to investigate the bulky chemical composition. The other part was used for the surface element composition analysis by XPS and the magnetic properties. The atomic ratio of Cu to Fe was both near to 1:2 in the fresh and used $CuFe_2O_4$ MNPs sample. However, the ratio of the elements on the surface of the fresh catalyst was found to be 1.16:1 (Fig. 7a), suggesting that the fresh catalyst surface was somewhat abundant in Cu element. After being used five times, the surface Cu/Fe molar ratio was decreased to 0.82:1, indicating that Cu element in catalyst surface was preferentially to dissolve than Fe element in the reaction solution. The result was consistent with Cu and Fe leaching in the reaction solution. Moreover, the used $CuFe_2O_4$ MNPs showed a reduced saturation moment per unit mass (1.8 emu g^{-1}), being slightly less than 2.2 emu g^{-1} for the fresh catalyst. The remained magnetic saturation moment allows an easy magnetic recovery of the catalyst after its uses.

3.6. Activation mechanism of PMS on $CuFe_2O_4$ MNPs

Radical quenching tests were performed to identify the dominant radical species. The activation of PMS by metal ion may produce three main types of reactive radicals, namely sulfate, peroxy-sulfate, and hydroxyl radicals [25]. Due to its weak oxidizing ability ($E(SO_5^{\bullet-}/SO_4^{2-}) = 1.1$ V), peroxy-sulfate is usually considered not responsible for the degradation of organic pollutants [19]. Hydroxyl radical may be generated by reaction of sulfate radical with H_2O as proceeded in Eq. (3) [19].

$$SO_4^{\bullet-} + H_2O \rightarrow SO_4^{2-} + {}^{\bullet}OH + H^+ \quad (3)$$

To identify the major reactive radical species generated in the PMS/$CuFe_2O_4$ system, alcohols were added into reaction solution

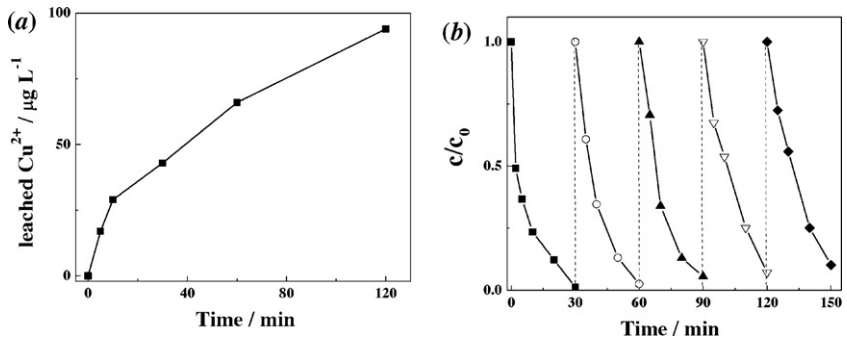

Fig. 6. (a) Leaching of Cu^{2+} from $CuFe_2O_4$ MNPs in neutral pH solutions with the addition of 0.5 g L^{-1} $CuFe_2O_4$ MNPs. (b) Degradation kinetics of TBBPA using the recycled catalysts. Reaction conditions: initial TBBPA concentration 10 mg L^{-1}, initial PMS concentration 0.2 mmol L^{-1}, catalyst load 0.1 g L^{-1}.

as quenching agents. Alcohols with and without α-hydrogen have different reactivity with radical species in different rates. Ethanol (EtOH, containing α-hydrogen) reacts with •OH or $SO_4^{\bullet-}$ at high and comparable rates, and the rate constants for the reactions with •OH and $SO_4^{\bullet-}$ are $(1.2–2.8)\times10^9$ mol L^{-1} s^{-1} and $(1.6–7.7)\times10^7$ mol L^{-1} s^{-1}, respectively [59]. However, tert-butyl alcohol (TBA, without α-hydrogen) has much different reaction rate constants with •OH or $SO_4^{\bullet-}$, and the rate constant for •OH ($(3.8–7.6)\times10^8$ mol L^{-1} s^{-1}) is 418–1900 times greater than that for $SO_4^{\bullet-}$ ($(4–9.1)\times10^5$ mol L^{-1} s^{-1}) [59]. Therefore, quenching tests were performed using either EtOH or TBA. As shown in Fig. 8, when no quenching agents were added, about 99% TBBPA was degraded in 30 min. However, the addition of 0.1 mol L^{-1} TBA and 0.1 mol L^{-1} EtOH resulted in decreasing TBBPA removal (in 30 min) to 92% and 78%, respectively. More addition of EtOH (0.2 mol L^{-1}) further decreased the TBBPA removal to 52%. The much more decrease of the TBBPA removal by EtOH than by TBA suggests that the main radical species generated during the activation of PMS by $CuFe_2O_4$ were sulfate radicals.

The proposed activation process of PMS by Fe^{3+} or Cu^{2+} was similar to that by Co^{2+}, which involves the generation of Fe^{2+} or Cu^{+} and the formation of $SO_4^{\bullet-}$ from the activation of PMS by the generated Fe^{2+} or Cu^{+} [18]. Therefore, the couples of PMS with homogeneous Fe^{2+}, Fe^{3+} and/or Cu^{2+} ions were used for wastewater treatment [41–45]. The present work confirmed that heterogeneous Fe_2O_3 and CuO nanoparticles could activate PMS and resulted in TBBPA removal of 66% and 85%, respectively (Fig. 3). Ji et al. reported phenol degradation by using PMS and CuO particles in aqueous solution and assumed that the activation of PMS was meditated by the redox pair of Cu(II)/Cu(I) [46]. Therefore, we speculate that the highly catalytic activity of $CuFe_2O_4$ MNPs involved the activation of PMS meditated by both redox pairs of Cu(II)/Cu(I) and Fe(III)/Fe(II) species in $CuFe_2O_4$ MNPs.

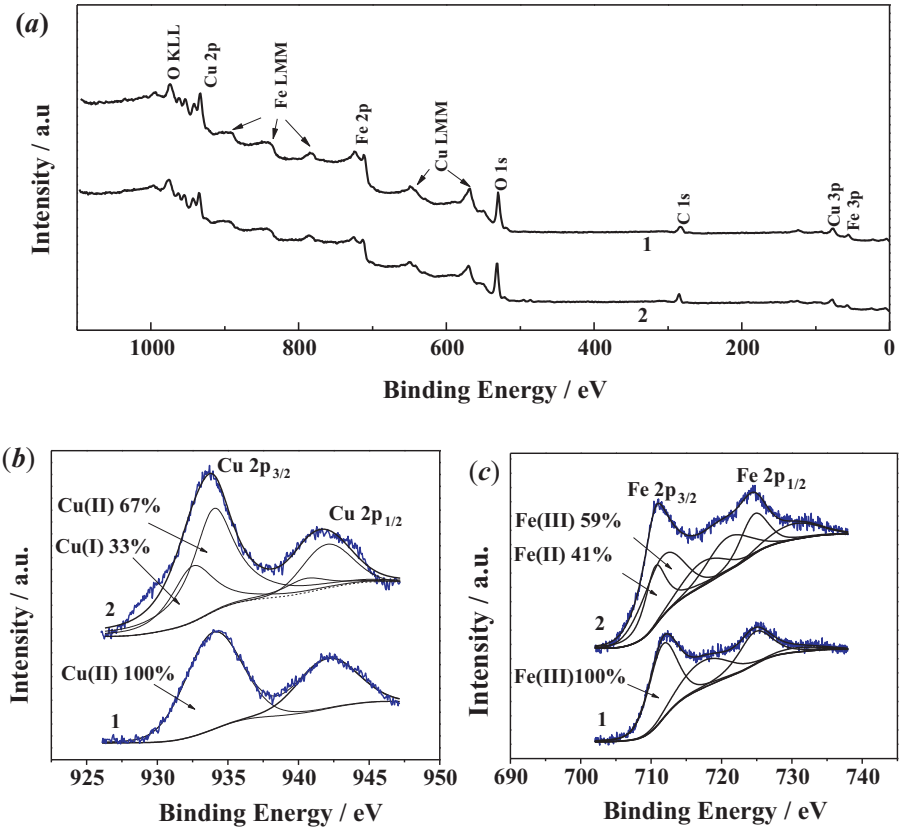

Fig. 7. (a) Wide survey XPS spectra and (b) Cu 2p and (c) Fe 2p XPS envelop of (1) the fresh and (2) used $CuFe_2O_4$ MNP catalysts.

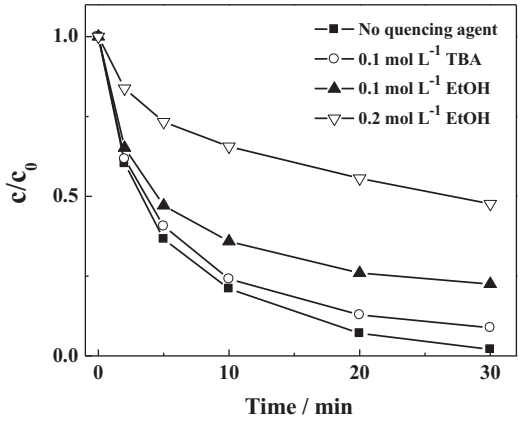

Fig. 8. Degradation kinetics of TBBPA in the system of PMS/$CuFe_2O_4$ without and with quenching agents of TBA (0.10 mol L^{-1}) and EtOH (0.10 and 0.20 mol L^{-1}). Reaction conditions: initial TBBPA concentration 10 mg L^{-1}, initial PMS concentration 0.2 mmol L^{-1}, and catalyst load 0.1 g L^{-1}.

To better understand the roles of Fe and Cu species in the activation of PMS, the XPS spectra of $CuFe_2O_4$ MNPs were recorded before and after the degradation experiment. As shown in Fig. 7b and c, the peaks of Cu 2p3/2 and Fe 2p3/2 were at 934.001 and 712.301 eV for the fresh $CuFe_2O_4$ MNPs catalyst, which were assigned to Cu(II) and Fe(III) [46,60]. These values slightly shifted to lower binding energy values (933.701 eV for Cu and 711.051 eV for Fe) after the catalytic degradation of TBBPA, which inferred that the valence of Cu and Fe species in the used catalyst was a mixture. Similar negative shift of binding energy value of 2p3/2 orbit was also reported by Ji et al. [46] and Deng et al. [61]. Deng et al. used $FeVO_4$ as a heterogeneous Fenton like catalyst for the degradation of Orange II in the presence of H_2O_2 and found that binding energy for Fe 2p3/2 declined from 711.19 eV in unused $FeVO_4$ to 710.91 eV in catalyst after 1 h of reaction. Based on the deconvolution of Cu (2p) and Fe (2p) envelop, Cu(I) and Fe(II) accounted for 33% and 41%, respectively, which indicated that Cu(II) and Fe(III) on surface of the used catalyst were transformed partially to Cu(I) and Fe(II), respectively.

According to the above experimental results, the mechanism of activation of PMS by $CuFe_2O_4$ catalyst was proposed as follows:

$$\equiv Cu^{2+} + HSO_5^- \rightarrow \equiv Cu^+ + SO_5^{\bullet -} + H^+ \quad (4)$$

$$\equiv Cu^+ + HSO_5^- \rightarrow \equiv Cu^{2+} + SO_4^{\bullet -} + OH^- \quad (5)$$

$$\equiv Cu^+ + \equiv Fe^{3+} \rightarrow \equiv Cu^{2+} + \equiv Fe^{2+} \quad (6)$$

$$\equiv Fe^{3+} + HSO_5^- \rightarrow \equiv Fe^{2+} + SO_5^{\bullet -} + H^+ \quad (7)$$

$$\equiv Fe^{2+} + HSO_5^- \rightarrow \equiv Fe^{3+} + SO_4^{\bullet -} + OH^- \quad (8)$$

According to the work of Nie et al. [62], the reduction of Fe^{3+} by Cu^+ (reaction (6)) is thermodynamically favorable as shown in the following equations:

$$Cu^{2+} + e^- \rightarrow Cu^+ \quad E^0 = 0.17\,V \quad (9)$$

$$Fe^{3+} + e^- \rightarrow Fe^{2+} \quad E^0 = 0.77\,V \quad (10)$$

The generated $\equiv Cu^+$ not only produces $SO_4^{\bullet -}$ through reaction (5), but also generates more $\equiv Fe^{2+}$ species on the surface of $CuFe_2O_4$, enhancing reaction (6). This electron transfer from Cu(I) to Fe(III) within the $CuFe_2O_4$ particles was supported by the lower content of Cu(I) (33%) than that of Fe(II) (41%). The electron transfer process was also reported with other inverse spinel ferrites such as $MnFe_2O_4$ during the photoassisted activation of H_2O_2 for the degradation of dye pollutants [63].

$$SO_4^{\bullet -} + H_2O \rightarrow {}^{\bullet}OH + H^+ + SO_4^{2-} \quad (11)$$

$$SO_4^{\bullet -} + TBBPA \rightarrow TBBPA^{\bullet +} + SO_4^{2-} \quad (12)$$

$$TBBPA^{\bullet +} + H_2O \rightarrow (OH)TBBPA^{\bullet} + H^+ \quad (13)$$

$$^{\bullet}OH + TBBPA \rightarrow (OH)TBBPA^{\bullet} \quad (14)$$

$$(OH)TBBPA^{\bullet} \rightarrow \text{intermediate} \rightarrow CO_2 + H_2O + Br^- \quad (15)$$

Therefore, the activation mechanism of PMS on $CuFe_2O_4$ MNPs was concluded as followed. Firstly, the organic pollutant TBBPA was adsorbed on the surface of $CuFe_2O_4$ MNPs catalyst (about 8% of the added TBBPA was observed to be adsorbed on the surface of $CuFe_2O_4$ (0.1 g L^{-1})). Once PMS was added, peroxy-sulfate radicals were generated from PMS being activated by the unveiled activation sites including Cu(II) and Fe(III). And then the reduced Cu(I) and Fe(II) sites catalyzed the decomposition of PMS to sulfate radicals. The generated sulfate radicals reacted with TBBPA both adsorbed on the catalyst surface and dissolved in the bulk solution, leading to full degradation and substantial mineralization of TBBPA.

3.7. Reaction pathway of TBBPA degradation in the system of PMS-$CuFe_2O_4$ MNPs

When $SO_4^{\bullet -}$ radicals oxidize the organic pollutant TBBPA, one electron is transferred to the organics to produce TBBPA radical cation ($TBBPA^{\bullet +}$) (Eq. (12)). Then the generated $TBBPA^{\bullet +}$ reacts quickly with H_2O by the way of hydroxyl abstraction or addition reaction to generate (hydroxyl) TBBPA radicals $(OH)TBBPA^{\bullet}$ (Eq. (13)) [64]. In this way, TBBPA is degraded by $SO_4^{\bullet -}$ in the $CuFe_2O_4$/PMS system. From the time-dependent evolution of the HPLC diagrams for TBBPA oxidation in the $CuFe_2O_4$/PMS system (Fig. S8 in Supporting Information), it was observed that the peak of TBBPA was decreased in strength as function of reaction time. Accompanied with the degradation of TBBPA, some new peaks occurred, indicative of the generation of degradation intermediates.

About 19 intermediates were identified by using LC–MS. According to the total ion current (TIC) of LC–MS analysis for TBBPA and for the solution after TBBPA degradation for 40 min (Fig. S9 in Supporting Information), the MS spectrum of the reaction mixture at 0 min showed a deprotonated molecular ion peak at m/z 542.7 with the retention time of 7.2 min. It is ascribed to the parent compound of TBBPA in accordance with the formula of $C_{12}H_{12}Br_4O_2$ (M = 544). The TBBPA as commercial product is relatively pure, but there is always small amount of tribromobisphenol A (TriBBPA) at m/z 462.8 with the retention time of 5.9 min [13]. Upon degradation for 40 min, 13 intermediates were identified, including 9 dibrominated phenol species, 2 monobrominated phenol species and 2 short chain aliphatic acids (Table S1 in Supporting Information).

Among them, the products at m/z 309, m/z 293 and m/z 265 were formed through the cleavage between one of the benzene rings and the isopropyl group by the attack of $SO_4^{\bullet -}$ on the middle carbon atom. They were further transformed to the other three dibrominated phenol species and two monobrominated phenol species with m/z 328, m/z 325, m/z 281, m/z 216 and m/z 260 through hydroxylation and demethylation reactions. This is similar with the observation of Eriksson et al., who investigated the direct photolysis of TBBPA with UV irradiation in aqueous solution and proposed that the primary photochemical reaction involved cleavage of the middle carbon atom [13]. An intermediate 2,6-dibromo-4-isopropenylphenol with m/z 291 being usually detected in the previous reports about the degradation of TBBPA [8,10,13] was not detected in the present work, which is possibly due to its low concentration or its transformation to other intermediates such as those at m/z 309 and m/z 293.

In addition to the attack of $SO_4^{\bullet -}$ on the middle carbon atom, $SO_4^{\bullet -}$ also can directly substitute Br atom through debromination and hydroxylation, resulting in the benzene ring openness to

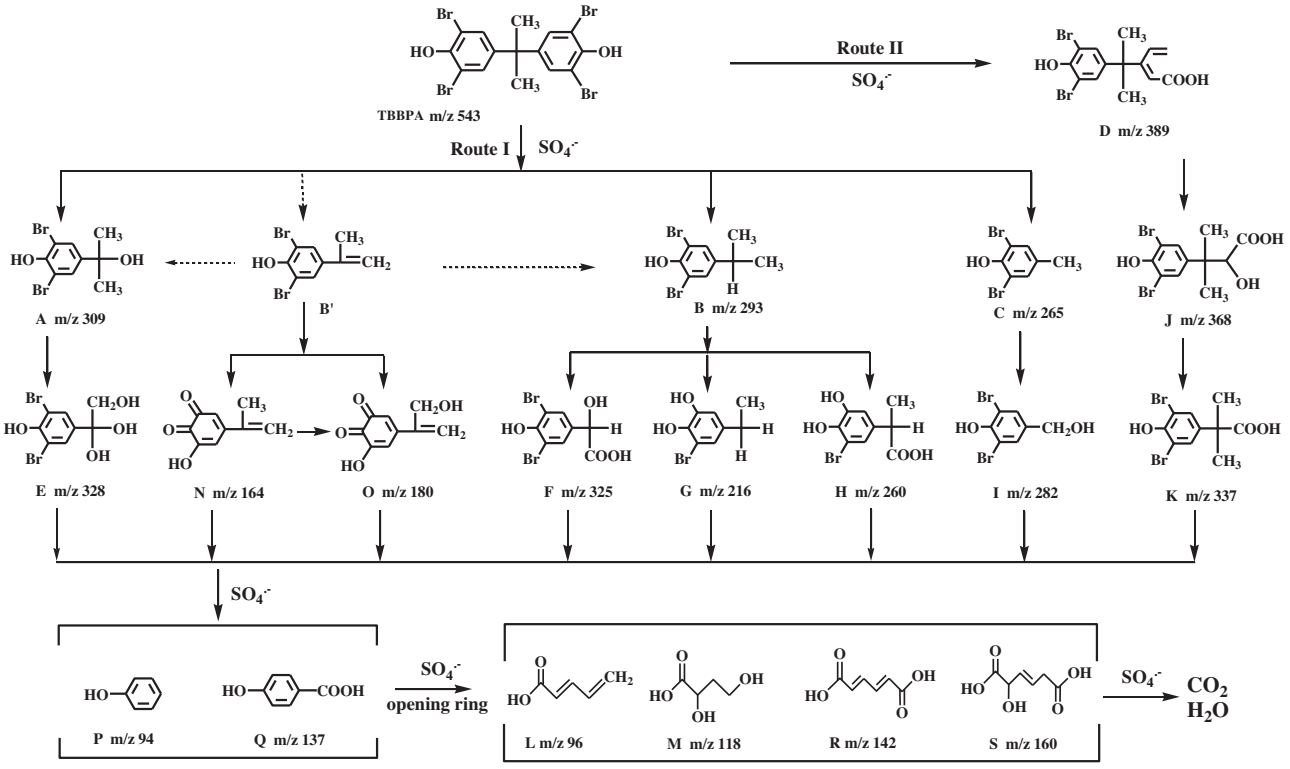

Scheme 1. Possible pathways of TBBPA degradation induced by sulfate radicals.

form (E)-3-(2-(3,5-dibromo-4-hydroxyphenyl)propan-2-yl)penta-2,4-dienoic acid with *m*/*z* 389. This product subjected further debrominaton and hydroxylation to produce two intermediates at *m*/*z* 368 and *m*/*z* 337. Similar intermediates were observed by Kabiersch and co-workers through one-electron oxidation of BPA by Mn^{3+} ions generated by purified neutral manganese peroxidase (MnP) from the litter-decomposing fungus [65]. However, these intermediates detected in the present study were different from the previously reported brominated compounds during the photochemical transformation of TBBPA under UV irradiation as well as in the oxidation of TBBPA by MnO_2 and solar-BiOBr photocatalysis due to the characteristics of $SO_4^{\bullet-}$ oxidation [8,10,13].

The degradation of these brominated compounds was of importance as they may have great potential threats to aqueous environment [15]. It was found that three main intermediates at *m*/*z* 309, *m*/*z* 328 and *m*/*z* 337 (Fig. S10 in Supporting Information) were first accumulated until reaching a maximum value, and then were degraded rapidly in the sequent reactions (Fig. S11 in Supporting Information). This indicates that the accumulation of the brominated intermediates is little in the investigated oxidative degradation system.

Beside the brominated products, the aromatic compounds and organic acids were also identified by the mass spectrometer (Agilent 1100 LC/MSD Trap, USA) in electrospray positive ion (ESI^+) mode with more polar elute of methanol and water (5:95, v/v). Four aromatic intermediates and another two short chain aliphatic acids were identified (Fig. S12 in Supporting Information). Similar intermediates were detected in the degradation of bisphenol A by using hemoglobin immobilized on amino modified magnetic nanoparticles as an enzyme catalyst [66], Ti-based PbO_2-ionic liquids electrode electrocatalyst [67] and nitrogen doped $K_2Nb_4O_{11}$ photocatalyst [68]. However, they have been not identified as intermediates of the direct oxidation of TBBPA before.

Based on the general rules of sulfate radical based oxidation [16–18,61], the referenced literature of TBBPA degradation in other reaction systems [8–14] and the experimental results in the study, we proposed the degradation pathway of TBBPA by $SO_4^{\bullet-}$ in the $CuFe_2O_4$/PMS system as shown in Scheme 1: $SO_4^{\bullet-}$ firstly attacked TBBPA to induce the degradation of TBBPA through two different routes of (I) the cleavage of central carbon of TBBPA and (II) substitution of Br atom by hydroxylation and debromination. The initial cleavage of central carbon of TBBPA gave three dibrominated products, **A**, **B**, **C**. The methyl group in compounds, **A**, **B**, **C** underwent a progressive transformation to aldehyde and carboxyl group to produce compounds, **E**, **F** and **I** (TBBPA → **A** → **E**; TBBPA → **B** → **F**; TBBPA → **C** → **I**). Or they underwent hydroxylation and debromination to produce monobrominated intermediates including compounds **G** and **H** (TBBPA → **B** → **G** and **H**). By the same pathway, intermediates **N** and **O** were produced from compound B' (TBBPA → **B**′ → **N**→**O**). Another compound **D** was produced through the second route (II) and further transformed to compounds **J** and **K** (TBBPA → **D** → **J** → **K**).

Further attack of $SO_4^{\bullet-}$ resulted in the generation of phenol (**P**), 4-hydroxybenzoic acid (**Q**) and four short chain aliphatic acids, **L**, **M**, **R** and **S** through the cleavage of the aromatic rings. Finally, the degradation of TBBPA was ended by the mineralization to CO_2 and H_2O.

4. Conclusions

$CuFe_2O_4$ MNPs were first used as a heterogeneous catalyst of PMS. It was found that $CuFe_2O_4$ MNPs posed a higher catalytic activity towards the degradation of TBBPA in the presence of PMS in comparison with Fe_2O_3 and CuO. 99% of 10 mg L^{-1} TBBPA could be degraded in 30 min by using 0.2 g L^{-1} $CuFe_2O_4$ MNPs to catalyze PMS (0.2 mmol L^{-1}). Complete degradation of TBBPA was achieved by using 1.5 mmol L^{-1} PMS, resulting in high TOC removal (56%) and debromination (67%) of TBBPA. XPS results indicated the highly catalytic activity could be attributed to a catalytic mechanism involving both Cu(II) and Fe(III) in $CuFe_2O_4$ MNPs. Based

on the LC–MS analysis of the degradation intermediates, a detail mechanism for TBBPA degradation was proposed. The mechanism indicates that TBBPA is able to not only be degraded, but also be debrominated and mineralized. Therefore, the activation of PMS by $CuFe_2O_4$ MNPs as a green oxidation process has promising potentials in the application in the field of pollution control.

Acknowledgments

This work was supported by the National Science Foundation of China (Grant Nos. 21077037 and 21177044), the National High Technology Research and Development Program of China (863 Program) (Grant No. 2012AA 06A 304), and Fundamental Research Funds for the Central Universities of China (Grant No. 2011TS121 and CZZ11008).

Appendix A. Supplementary data

Supplementary data associated with this article can be found, in the online version, at http://dx.doi.org/10.1016/j.apcatb.2012.09.015.

References

[1] C.A. de Wit, Chemosphere 46 (2002) 583–624.
[2] U. Sellström, B. Jansson, Chemosphere 31 (1995) 3085–3092.
[3] K. Öberg, K. Warman, T. Öberg, Chemosphere 48 (2002) 805–809.
[4] M.S.E. Mäkiene, M.R.A. Mäkiene, J.T.B. Koistinen, A.-L. Pasanen, P.J. Kalliokoski, A.M. Korpi, Environmental Science and Technology 43 (2009) 941–947.
[5] S. Kitamura, T. Suzuki, S. Sanoh, R. Kohta, N. Jinno, K. Sugihara, S. Yoshihara, N. Fujimoto, H. Watanabe, S. Ohta, Toxicological Sciences 84 (2005) 249–259.
[6] J.B. Fini, S.L. Mevel, N. Turque, K. Palmier, D. Zalko, J.P. Cravedi, B.A. Demeneix, Environmental Science and Technology 41 (2007) 5908–5914.
[7] J.W. Voordeckers, D.E. Fennell, K. Jones, M.M. Häggblom, Environmental Science and Technology 36 (2002) 696–701.
[8] K.D. Lin, W.P. Liu, J. Gan, Environmental Science and Technology 43 (2009) 4480–4486.
[9] Y.N. Guo, L. Chen, F.Y. Ma, S.Q. Zhang, Y.X. Yang, X. Yuan, Y.H. Guo, Journal of Hazardous Materials 189 (2011) 614–618.
[10] J. Xu, W. Meng, Y. Zhang, L. Li, C.S. Guo, Applied Catalysis B 107 (2011) 355–362.
[11] S.K. Han, R.H. Sik, A.G. Motten, C.F. Chignell, P.J. Bilski, Photochemistry and Photobiology 85 (2009) 1299–1305.
[12] S.K. Han, P.J. Bilski, B.K. arriker, R.H. Sik, C.F. Chignell, Environmental Science and Technology 42 (2008) 166–172.
[13] J. Eriksson, S. Rahm, Ni Green, Å. Bergman, E. Jakobsson, Chemosphere 54 (2004) 117–126.
[14] S. Luo, S.G. Yang, C. Sun, X.D. Wang, Water Research 45 (2011) 1519–1528.
[15] E. Bruchajzer, J.A. Szymanska, J.K. Piotrowski, Toxicology Letters 134 (2002) 245–252.
[16] H. Hori, A. Yamamoto, E. Hayakawa, S. Taniyasu, N. Yamashita, S. Kutsuna, Environmental Science and Technology 39 (2005) 2383–2388.
[17] S.Y. Yang, P. Wang, X. Yang, L. Shan, W.Y. Zhang, X.T. Shao, R. Niu, Journal of Hazardous Materials 179 (2010) 552–558.
[18] G.P. Anipsitakis, D.D. Dionysiou, Environmental Science and Technology 38 (2004) 3705–3712.
[19] G.P. Anipsitakis, D.D. Dionysiou, Environmental Science and Technology 37 (2003) 4790–4797.
[20] X. Chen, X. Qiao, D. Wang, J. Lin, J. Chen, Chemosphere 67 (2007) 802–808.
[21] Y.H. Huang, Y.F. Huang, C.I. Huang, C.Y. Chen, Journal of Hazardous Materials 170 (2009) 1110–1118.
[22] G.P. Anipsitakis, D.D. Dionysiou, M.A. Gonzalez, Environmental Science and Technology 40 (2006) 1000–1007.
[23] G.P. Anipsitakis, T.P. Tufano, D.D. Dionysiou, Water Research 42 (2008) 2899–2910.
[24] S.H. Do, J.H. Jo, Y.H. Jo, H.K. Lee, S.H. Kong, Chemosphere 77 (2009) 1127–1131.
[25] M. Pagano, A. Volpe, G. Mascolo, A. Lopez, V. Locaputo, R. Cianarella, Chemosphere 85 (2012) 329–334.
[26] D. Lison, CRC Critical Reviews in Toxicology 26 (1996) 585–616.
[27] G.P. Anipsitakis, E. Stathatos, D.D. Dionysiou, Journal of Physical Chemistry C 109 (2005) 13052–13055.
[28] X. Chen, J. Chen, X. Qiao, D. Wang, X. Cai, Applied Catalysis B 80 (2008) 116–121.
[29] Q.J. Yang, H. Choi, D.D. Dionysiou, Applied Catalysis B 74 (2007) 170–178.
[30] L. Hu, X. Yang, S. Dang, Applied Catalysis B 102 (2011) 19–26.
[31] W. Zhang, H. Tay, S. Lim, Y. Wang, Z. Zhong, R. Xu, Applied Catalysis B 95 (2010) 93–99.
[32] P. Shukla, S. Wang, K. Singh, H.M. Ang, M.O. Tadé, Applied Catalysis B 99 (2010) 163–169.
[33] P. Shukla, S. Wang, H. Sun, H.M. Ang, M.O. Tadé, Applied Catalysis B 100 (2010) 529–534.
[34] Y. Hardjono, H. Sun, H. Tian, C.E. Buckley, S. Wang, Chemical Engineering Journal 174 (2011) 376–382.
[35] P.H. Shi, R.J. Su, S.B. Zhu, M.C. Zhu, D.X. Li, S.H. Xu, Journal of Hazardous Materials 229–230 (2012) 331–339.
[36] P.H. Shi, R.J. Su, F.Z. Wan, M.C. Zhu, D.X. Li, S.H. Xu, Applied Catalysis B 123–124 (2012) 265–272.
[37] S. Muhammad, E. Saputra, H.Q. Sun, J. de, C. Izidoro, D.A. Fungaro, H.M. Ang, M.O. Tadé, S.B. Wang, RSC Advances 2 (2012) 5645–5650.
[38] Y.B. Ding, L.H. Zhu, A.Z. Huang, X.R. Zhao, X.Y. Zhang, H.Q. Tang, Catalysis Science & Technology 2 (2012) 1977–1984.
[39] Q.J. Yang, H. Choi, S.R. Al-Abed, D.D. Dionysiou, Applied Catalysis B 88 (2009) 462–469.
[40] Y.J. Yao, Z.H. Yang, D.W. Zhang, W.C. Peng, H.Q. Sun, S.B. Wang, Industrial and Engineering Chemistry Research 51 (2012) 6044–6051.
[41] A. Rastogi, S.R. Ai-Abed, D.D. Dionysiou, Applied Catalysis B 85 (2009) 171–179.
[42] Y.R. Wang, W. Chu, Journal of Hazardous Materials 186 (2011) 1455–1461.
[43] Y.R. Wang, W. Chu, Applied Catalysis B 123–124 (2012) 151–161.
[44] J. Madhavan, P. Maruthamuthu, S. Murugesan, S. Anandan, Applied Catalysis B 83 (2008) 8–14.
[45] P. Nfodzo, H. Choi, Chemical Engineering Journal 174 (2011) 629–634.
[46] F. Ji, C. Li, L. Deng, Chemical Engineering Journal 178 (2011) 239–243.
[47] M. Sugimoto, Journal of the American Ceramic Society 82 (1999) 269–280.
[48] W.F. Shangguan, Y. Teraoka, S. Kagawa, Applied Catalysis B 16 (1998) 149–154.
[49] M. Estrella, L. Barrio, G. Zhou, X. Wang, Q. Wang, W. Wen, J.C. Hanson, A.I. Frenkel, J.A. Rodriguez, Journal of Physical Chemistry C 113 (2009) 14411–14417.
[50] K. Faungnawakij, N. Shimoda, T. Fukunaga, R. Kikuchi, K. Eguchi, Applied Catalysis B 92 (2009) 341–350.
[51] R. Wu, J. Qu, H. He, Y. Yu, Applied Catalysis B 48 (2004) 49–56.
[52] P. Laokul, V. Amornkitbamrung, S. Seraphin, S. Maensiri, Current Applied Physics 11 (2011) 101–108.
[53] Y. Tanaka, R. Kikuchi, T. Takeguchi, K. Eguchi, Applied Catalysis B 57 (2005) 211–222.
[54] J.H. Xu, H. Ke, D.C. Jia, W. Wang, Y. Zhou, Journal of Alloys and Compounds 472 (2009) 473–477.
[55] S. Ayyappan, J. Philip, B. Raj, Journal of Physical Chemistry C 113 (2009) 590–596.
[56] J.E. Tasca, C.E. Quincoces, A. Lavat, A.M. Alvarez, M.G. González, Ceramics International 37 (2011) 803–812.
[57] P. Shukla, H. Sun, S. Wang, H.M. Ang, M.O. Tadé, Catalysis Today 175 (2011) 380–385.
[58] P. Shukla, H. Sun, S. Wang, H.M. Ang, M.O. Tadé, Separation Science and Technology 77 (2011) 230–236.
[59] C.J. Liang, H.W. Su, Industrial and Engineering Chemistry Research 48 (2009) 5558–5562.
[60] I. Nedkov, R.E. Vandenberghe, T. Marinova, P. Thailhades, T. Merodiiska, I. Avramova, Applied Surface Science 253 (2006) 2589–2596.
[61] J.H. Deng, J.Y. Jiang, Y.Y. Zhang, X.P. Lin, C.M. Du, Y. Xiong, Applied Catalysis B 84 (2008) 468–473.
[62] Y.L. Nie, C. Hu, J.H. Qu, X. Zhao, Applied Catalysis B 87 (2009) 30–36.
[63] B. Sahoo, S.K. Sahu, S. Nayak, D. Dharaa, P. Pramanik, Catalysis Science & Technology 2 (2012) 1367–1374.
[64] J.C. Yan, M. Lei, L.H. Zhu, M.N. Anjum, J. Zou, H.Q. Tang, Journal of Hazardous Materials 186 (2011) 1398–1404.
[65] G. Kabiersch, J. Rajasärkkä, R. Ullrich, M. Tuomela, M. Hofrichter, M. Virta, A. Hatakka, K. Steffen, Chemosphere 83 (2011) 226–232.
[66] T.T. Tang, H. Fan, S.Y. Ai, R.X. Han, Y.Y. Qiu, Chemosphere 83 (2011) 255–264.
[67] P. Ju, H. Fan, D.D. Guo, X.M. Meng, M.R. Xu, S.Y. Ai, Chemical Engineering Journal 179 (2012) 99–106.
[68] Y.F. Qiu, L. Wang, C.F. Leung, G.J. Liu, S.H. Yang, T.C. Lau, Applied Catalysis A 402 (2011) 23–30.